EARTH SURFACE PROCESSES AND LANDFORMS
Earth Surf. Process. Landforms (2017)

Published online in Wiley Online Library
(wileyonlinelibrary.com) DOI: 10.1002/esp.4235

The effect of tides and storms on the sediment transport across a Dutch barrier island

Daan Wesselman,[1]* Renske de Winter,[1] Anita Engelstad,[1] Robert McCall,[2] Ap van Dongeren,[2] Piet Hoekstra,[1] Albert Oost[2] and Maarten van der Vegt[1]
[1] Department of Physical Geography, Faculty of Geosciences, Utrecht University, Utrecht, The Netherlands
[2] Deltares, Boussinesqweg 1, Delft, The Netherlands

Received 9 March 2017; Revised 7 July 2017; Accepted 21 August 2017

*Correspondence to: Daan Wesselman, Department of Physical Geography, Faculty of Geosciences, Utrecht University, Utrecht, The Netherlands. E-mail: d.a.wesselman@uu.nl

ESPL
Earth Surface Processes and Landforms

ABSTRACT: Under natural conditions, barrier islands might grow vertically and migrate onshore under the influence of long-term sea level rise. Sediment is transported onshore during storm-induced overwash and inundation. However, on many Dutch Wadden Islands, dune openings are closed off by artificial sand-drift dikes that prevent the influx of sediment during storms. It has been argued that creating openings in the dune row to allow regular flooding on barrier islands can have a positive effect on the sediment budget, but the dominant hydrodynamic processes and their influence on sediment transport during overwash and inundation are unknown. Here, we present an XBeach model study to investigate how sediment transport during overwash and inundation across the beach of a typical mesotidal Wadden Sea barrier island is influenced by wave, tide and storm surge conditions. Firstly, we validated the model XBeach with field data on waves and currents during island inundation. In general, the XBeach model performed well. Secondly, we studied the long-term sediment transport across the barrier island. We distinguished six representative inundation classes, ranging from frequently occurring, low-energy events to infrequent, high-energy events, and simulated the hydrodynamics and sediment transport during these events. An analysis of the model simulations shows that larger storm events cause larger cross-shore sediment transport, but the net sediment exchange during a storm levels off or even becomes smaller for the largest inundation classes because it is counteracted by larger mean water levels in the Wadden Sea that oppose or even reverse sediment transport during inundation. When taking into account the frequency of occurrence of storms we conclude that the cumulative effect of relatively mild storms on long-term cross-shore sediment transport is much larger than that of the large storm events. © 2017 The Authors. Earth Surface Processes and Landforms published by John Wiley & Sons Ltd.

KEYWORDS: barrier islands; inundation; hydrodynamics; sediment transport; XBeach

Introduction

Many barrier systems all over the world are threatened by the effects of long-term sea level rise (Flato *et al.*, 2013). If sediment is abundant and the rate of sea level rise is small, barrier islands can maintain their shape by moving landward, a process called rollover (Donnelly *et al.*, 2006; Leatherman, 1985; Masselink and van Heteren, 2014; Williams, 2015). The landward transport of sediment can take place during overwash and inundation, which typically occurs during storm surge conditions. During the overwash regime, waves overtop the maximum barrier island height (i.e. the beach or dune crest), whereas during the inundation phase the water level also exceeds the island crest (Sallenger, 2000). The associated gradients in sediment transport can result in vertical accretion of barriers by sediment deposited landward in the form of washover fans and terraces (Hoekstra *et al.*, 2009; Leatherman, 1976; Masselink and van Heteren, 2014).

Existing studies on overwash and inundation often focused on microtidal regimes and narrow barrier islands with hurricane-driven wind and wave conditions or morphology change after a storm (i.e. the end product: the post-storm morphology) rather than the processes during overwash and inundation itself (Donnelly *et al.*, 2004; FitzGerald *et al.*, 2007; McCall *et al.*, 2010; Morton and Sallenger, 2003; Plant and Stockdon, 2012; Schupp *et al.*, 2013; Williams, 2015). Hurricane-driven storms typically result in a large wind set-up (Androulidakis *et al.*, 2015) and wave set-up (Lazarus and Armstrong, 2015; Longuet-Higgins, 1983). Here, strong erosion of the dunes or even breaching of the barrier islands can occur during overwash and inundation. The scarce studies on overwash and inundation processes at barriers in mesotidal, extra-tropical conditions focused on the influence of island geometries on the occurrence of overwash and inundation (Matias *et al.*, 2009) or on morphological change after a storm (e.g. Nielsen and Nielsen, 2006), but the underlying processes have not been studied in detail yet (Lazarus, 2016). One of the reasons for this is that it is difficult to measure the hydrodynamics and sediment transport during storm conditions (Donnelly *et al.*, 2006; Van Dusen *et al.*, 2016). To develop

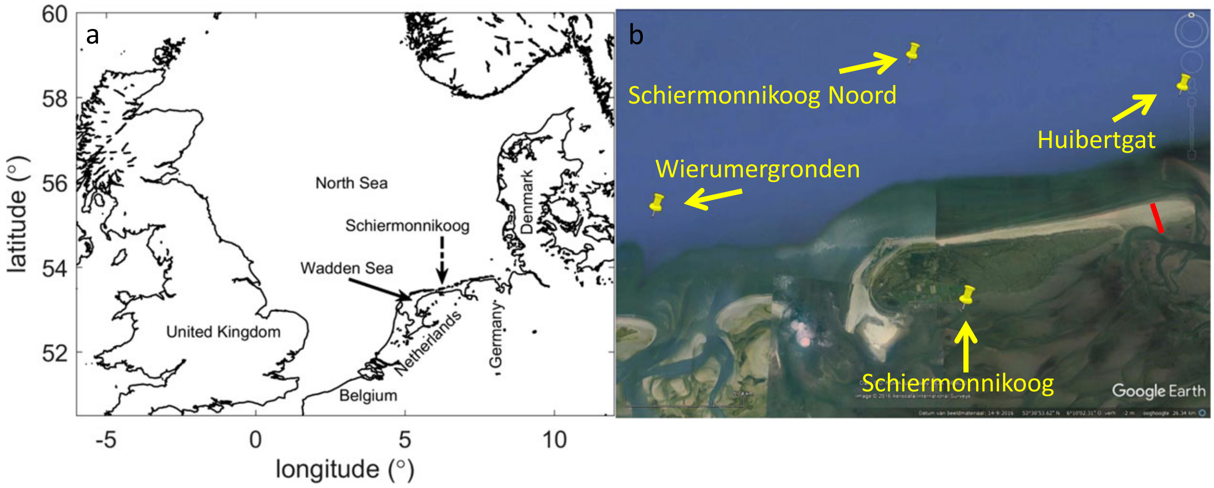

Figure 1. (a) The Wadden area in the Netherlands, Germany and Denmark, including the North Sea, barrier islands, tidal inlets and a series of tidal basins (Wadden Sea). The dashed arrow indicates the Wadden Island Schiermonnikoog, Netherlands. (b) Schiermonnikoog in more detail. The red line is the location of the cross-shore field array. Schiermonnikoog Noord is a wave buoy; Wierumergronden, Huibertgat and Schiermonnikoog are water level stations. [Colour figure can be viewed at wileyonlinelibrary.com]

a better understanding of the role of overwash and inundation processes on the vertical accretion of barriers, insight into hydrodynamic processes and sediment transport during these regimes is crucial (Lapetina and Sheng, 2015), and this knowledge should preferably be developed based on field studies interacting with process-based models.

Here, we focus on the barrier islands in the Wadden Sea, which are exposed to a mesotidal environment (a tidal range of 2–4 m, depending on the location) characterized by strong autumn and winter storms that generate waves and storm surges in the North Sea. The Wadden area along the coast of the Netherlands, Germany and Denmark is a chain of barrier islands, tidal inlets and back-barrier basins (Figure 1a). Typical Wadden Island beaches are wide and slope relatively gently (Hoekstra *et al.*, 2009). The barrier islands have a typical drumstick shape (Hayes, 1979). The Wadden Islands are examples of barrier islands that can experience overwash and inundation during storm events (Hoekstra *et al.*, 2009). The characteristic North Sea and Wadden Sea wave, tide and storm surge conditions affect sediment transport during overwash and inundation. The storms in the Wadden area can result in severe wave and wind set-up. The combination of wave- and wind-induced set-up and tidal variations, both in the North Sea and Wadden Sea, affects the magnitude and direction of the flow velocity across the island in the inundation regime (Engelstad *et al.*, 2017; Harter and Figlus, 2017; Hoekstra *et al.*, 2009; Sherwood *et al.*, 2014). The short waves (<20 s) move to the shore in wave groups, creating infragravity (IG) waves with a period of 20–200 s (Battjes, 1974; Herbers *et al.*, 1994; Longuet-Higgins and Stewart, 1962). These IG waves have been found to be important on gentle slopes such as those of the Wadden Islands (de Bakker *et al.*, 2015), which enhances the stirring and transport of sediment (Beach and Sternberg, 1988). For gentle sloping, dissipative Wadden coasts the importance of these hydrodynamic processes for sediment transport during overwash and inundation have not been studied so far. Furthermore, no research has been done yet on the role of relatively small, more frequently occurring North Sea storms versus larger, exceptional storms.

The aim of this study is twofold. The first aim is to validate the 1D version of the process-based model XBeach for hydrodynamic processes (i.e. water levels, short and IG wave heights and flow velocities) during overwash and inundation for North Sea conditions. XBeach includes all these processes and is therefore a useful tool to analyse hydrodynamics and the resulting sediment transport during overwash and inundation (Roelvink *et al.*, 2009). To this end, we gathered a unique field-data set at the island tail of Schiermonnikoog, where we measured these hydrodynamic parameters during several overwash and inundation events over 3 months in the winter of 2014–2015. The second aim is to extend our knowledge on hydrodynamic processes and sediment transport during overwash and inundation for mesotidal conditions. This is done by using the validated XBeach model. To reach this aim, we investigate how sediment transport during overwash and inundation across the beach of a typical Wadden Sea barrier island is influenced by wave, tide and storm surge conditions. Subsequently, we study the potential decadal overwash- and inundation- induced sediment transport across the barrier island.

Methods

Field data

Data on the hydrodynamics are obtained during a measurement campaign at the Eastern tip of the barrier island Schiermonnikoog, the Netherlands (Figure 1b), from 4 November 2014 to 31 January 2015. The field data are used to validate the XBeach model. Overwash and inundation can take place at several locations along the island (Figure 2). The so-called washover openings – gaps between the dunes – are typically below 2.0 m above mean sea level (MSL) and will be flooded during storm conditions. Furthermore, the island tail lacks dunes completely and has a beach crest at 1.6 m above MSL (i.e. the highest point of the cross-shore profile), which means that it will be inundated completely several times a year. This island tail is chosen for our field campaign for two reasons. Firstly, the beach crest is approximately 20–30 cm lower than many washover openings closer to the updrift side, which makes the chance of actually measuring overwash and inundation events at this site higher. Secondly, beach morphology and nearshore bathymetry are almost uniform in the alongshore direction and vegetation is lacking. The alongshore uniform conditions are ideal to validate the XBeach model, since the focus will be on the dominant cross-shore patterns. The foreshore has a very mild slope (1:100), with three offshore bars (Figure 3a). The beach crest is located a few hundred meters onshore, and inland of the beach crest the barrier height gradually decreases (Figure 3b). The offshore high-water levels range between 0.7 m above MSL at neap tide

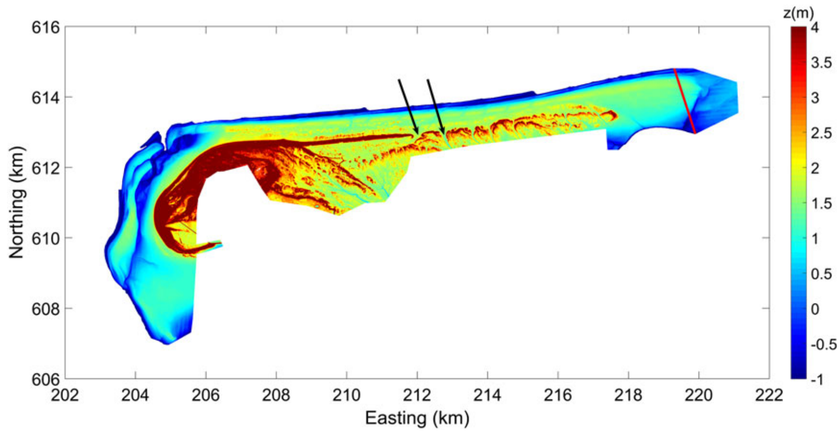

Figure 2. A lidar image from Schiermonnikoog, 2002. The colour represents the height and the red line shows the location of the field area. The height corresponds to MSL. The black arrows indicate the two most updrift washover openings. Coordinates are given in the local RD2008 system. [Colour figure can be viewed at wileyonlinelibrary.com]

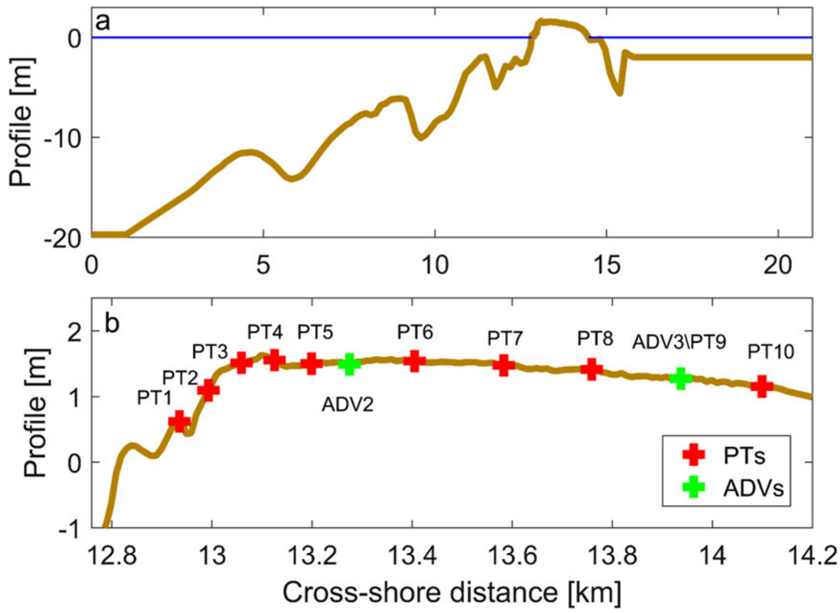

Figure 3. (a) Schiermonnikoog cross-shore profile. North Sea is to the left, Wadden Sea to the right. The blue line represents MSL. (b) Locations of the instruments during the field campaign at Schiermonnikoog. Two ADVS are placed and 10 PTs. [Colour figure can be viewed at wileyonlinelibrary.com]

and 1.2 m above MSL at spring tide, while the highest storm surge level in the last 25 years is 3.5 m. In the Discussion section a brief elaboration will be given on the potential differences during overwash and inundation between the island tail and the washover openings.

Ten stand-alone pressure transducers (PT; Ocean Sensor Systems Wave Gauges, OSSI-010-003C) and two instrument rigs containing an acoustic Doppler velocimeter (ADV; Nortek Vector, cabled version) are installed in a cross-shore array from the North Sea side to the Wadden Sea side of Schiermonnikoog (Figure 3b). The PTs record at 10 Hz, continuously. While fully submerged, the PTs measure mean water levels and water level variations. The ADVs measure flow velocities, recorded at 16 Hz, and are located 13–17 cm above the bed. Water levels (Z), water depth (h) and flow velocities (u) are decomposed into a cross-shore and alongshore component and averaged over 15 min. Short and IG wave heights are determined from the variance of the second-order detrended sea surface elevation, using a highpass filter (0.05–1 Hz) and a lowpass filter (0.005–0.05 Hz). The bed profile of the intertidal and subtidal part of the profile is measured with a RTK-dGPS system at the beginning and at the end of the field campaign. The offshore bed-level profile is obtained from Vaklodingen (annual depth and height measurements of the Dutch sandy coast) and merged with the measured island profile.

Water level data are available at 10 min intervals in the North Sea and Wadden Sea and are obtained from the Rijkswaterstaat (RWS; part of the Dutch Ministry of Infrastructure and the Environment). For the North Sea, the water level stations Wierumergronden and Huibertgat are used, and for the Wadden Sea it is the station Schiermonnikoog (Figure 1b). Hourly data on significant short wave height (H_s), peak period (T_p), wave direction (D) and directional spreading are obtained from the wave buoy Schiermonnikoog Noord, which is located at a water depth of approximately 20 m. Additionally, for the inundation events during the field campaign, directional wave spectra for every 3 h are obtained from RWS.

XBeach

In this study, we use XBeach (Kings Day release) for the modelling of hydrodynamic processes and sediment transport during overwash and inundation for North Sea storm conditions.

XBeach is a process-based numerical model developed to simulate storm events, and it includes the impact of overwash and inundation. The model has been shown to predict storm-driven morphological change well (McCall *et al.*, 2010; de Winter *et al.*, 2015). Furthermore, the studies of Stockdon *et al.* (2014) and de Winter *et al.* (2015) demonstrated that wave run-up and wave height in the swash and collision regime can be simulated accurately. We refer to the Appendix for an overview of the governing equations regarding hydrodynamics and sediment transport, and to Roelvink *et al.* (2009) for a full description of the XBeach model.

The simulations consist of two parts. In the first part XBeach is validated with the field data; in the second part the various storm simulations are performed. XBeach is run in 1D mode and the cross-shore bed level profile from Figure 3a is used for all simulations. The grid size gradually changes from 20 m offshore to 2 m in shallow water. The prescribed offshore boundary conditions consist of water level data from offshore stations. The tide propagates along the shore from west to east, and the tidal amplitude increases. Therefore, the water level used for the validation run is determined by linearly interpolating the water level data at Wierumergronden and Huibertgat, the two nearest stations. At the Wadden Sea boundary, tidal water levels are prescribed with data from the Schiermonnikoog tidal station for all simulations. Wave forcing at the offshore boundary is prescribed using measured directional wave spectra for the validation runs, and JONSWAP spectral parameters (significant wave height, peak wave period, mean wave direction and directional spreading) for the other storm simulations. The wave data are obtained from the offshore buoy Schiermonnikoog Noord. To aid the representation of observed IG waves in the 1D XBeach cross-shore transect model, oblique waves at the boundary are rotated to the shore-normal direction before being imposed in the model. To compensate for the expected overestimation of the short- and IG wave heights, a refraction coefficient is applied as explained in Holthuijsen (2007), which compensates for the energy loss of oblique waves from deep water to the breaking zone. The breaking formulation 'Roelvink2' is used (Roelvink, 1993), where the breaking parameter gamma is set to 0.45 for all simulations instead of the default value of 0.55, which improved the model–data comparison. This is in line with Hoonhout and van Thiel de Vries (2012), where a gamma of 0.45 yielded better results for profiles with a gentle foreshore slope. The D50 of the sediment is 200 μm and the D90 is 300 μm. At the offshore and onshore boundary, the cross-shore suspended sediment transport gradients are set to zero. Each run is preceded by a spin-up period of one tidal cycle of 12.5 h and constant wave conditions, based on the first values of the actual simulation. The XBeach simulations are performed in morphostatic mode, which means that although sediment concentrations and transport are computed it does not lead to morphology change. The minor morphology change at the field site during the campaign allowed us to use this mode for the validation simulations. For all model parameters not mentioned here default values are used.

The following model data output (every second) is analysed: water depth (h), flow velocity (u), significant short wave height (H_s), sediment concentration and sediment transport. From the water level data, IG wave heights are calculated in the same way as from the field data. To calculate all mean values, the output is averaged over 15 min.

Model validation

We aim to validate the hydrodynamics in XBeach during overwash and inundation with the collected field data. For this goal, the squared correlation coefficient (r^2) and bias are calculated for all PTs (i.e. water levels, and short and IG wave heights) and ADVs (flow velocities) with Eqs. (1) and (2), respectively:

$$r^2 = \frac{\left[\sum_{i=1}^{n}(P_{\mathrm{model},i} - \bar{P}_{\mathrm{model}}) * (P_{\mathrm{data},i} - \bar{P}_{\mathrm{data}})\right]^2}{\sum_{i=1}^{n}(P_{\mathrm{model},i} - \bar{P}_{\mathrm{model}})^2 * \sum_{i=1}^{n}(P_{\mathrm{data},i} - \bar{P}_{\mathrm{data}})^2} \tag{1}$$

$$\mathrm{bias} = \frac{\sum_{i=1}^{n}(P_{\mathrm{model},i} - P_{\mathrm{data},i})}{n} \tag{2}$$

Here, n is the number of data points and P is one of the parameters used for the validation. Eleven overwash and inundation events are measured, varying in magnitude, wind direction and duration, and are all used for the validation. All events occurred between 11 December 2014 and 29 January 2015 (Engelstad *et al.*, 2017). Figure 4a shows, as an example, the water level curve of the inundation event with the highest measured water level during the campaign, together with the tidal cycles before and after the largest one. This storm occurred on 10 and 11 January 2015. The first tidal cycle contains a tidal phase lag between the North Sea and Wadden Sea. During the second and third tidal cycle, the mean and peak water levels in the Wadden Sea are larger than in the North Sea. During the entire period of 36 h, the offshore wave height varied between 2.5 and 6.9 m and the wave period between 5.0 and 9.5 s. The wave direction gradually changed from SW to NW (Figure 4b–d).

Long-term sediment transport

To study the contribution of overwash and inundation to sediment transport across the island, we analyse the net sediment transport at the beach crest, the highest point of the profile, because this sediment that is transported over the beach crest during overwash and inundation potentially becomes available for deposition on the island. To calculate the sediment transport across the beach crest for the long term (here we consider 25 years), three steps are taken. Firstly, an inundation classification scheme is developed (next section) based on the peak water level during a tidal cycle. This scheme represents the typical North Sea storms at Schiermonnikoog, ranging from gentle, frequently occurring storms (class 1) to large, high-energetic storms (class 6). Secondly, those inundation classes are simulated with XBeach, so that the typical hydrodynamic processes and their influence on sediment transport across the Wadden Island can be analyzed. Lastly, the total sediment transport per class is multiplied by the frequency of occurrence. In this way it can be analyzed how each class of storms contributes to the total sediment transport at the beach crest.

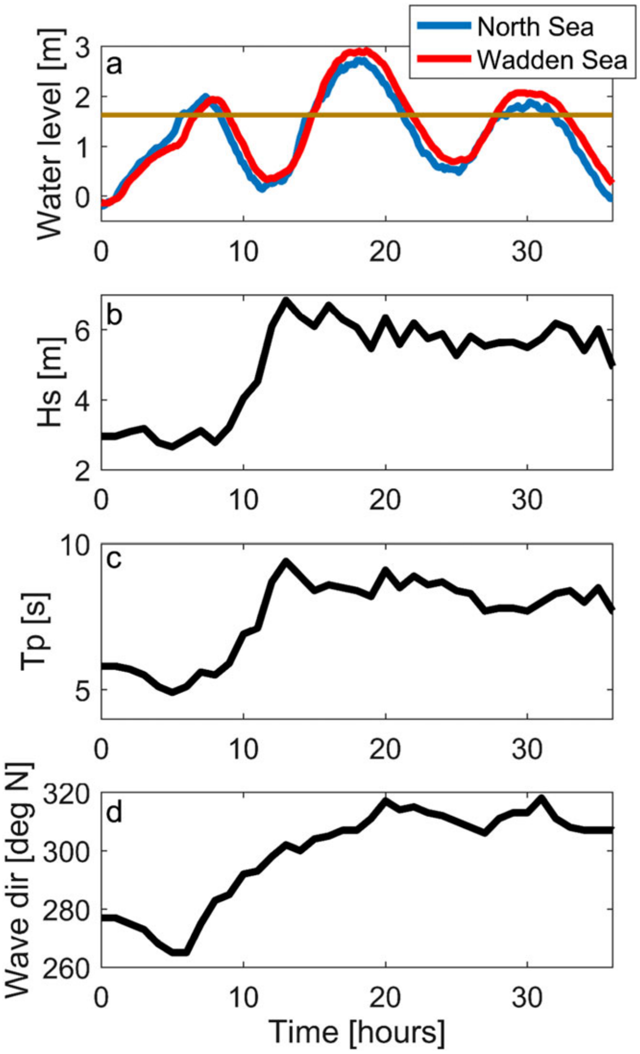

Figure 4. Three out of 11 inundation events in the North Sea and Wadden Sea as a function of time, used as boundary conditions for the validation runs. These three tidal cycles are from 10 January 7 am, to 11 January 7 pm., 2015 (a) Water level curves. The brown line represents the height of the beach crest. (b) Significant wave height. (c) Wave period. (d) Wave direction. [Colour figure can be viewed at wileyonlinelibrary.com]

Inundation classes

We categorize the measured storms and resulting water levels into what we call inundation classes. The aim of the inundation classification is to study the effect of different storm types in a systematic way based on storm records of the last 25 years, from 1990 to 2014. The inundation classes give an overview of the dominant hydrodynamic patterns and their influence on sediment transport across the island during inundation. The classification procedure for the water levels is illustrated in Figure 5.

The classes are based on the peak water level in the North Sea (station Huibertgat) during an inundation event. An inundation event is defined as a single tidal cycle with an offshore peak water level of at least 1.50 m above MSL. Peak values lower than 1.50 m hardly result in overwash or inundation based on the selected profile of Schiermonnikoog, and are therefore not included. The considered offshore peak water levels range from 1.50 m to a maximum of 3.00 m, with a separation of 0.25 m per class. Thus class 1 contains all individual inundation events with a peak water level in the North Sea between 1.50 and 1.75 m, and so forth. Owing to our definition of an inundation event, there can be multiple events in a

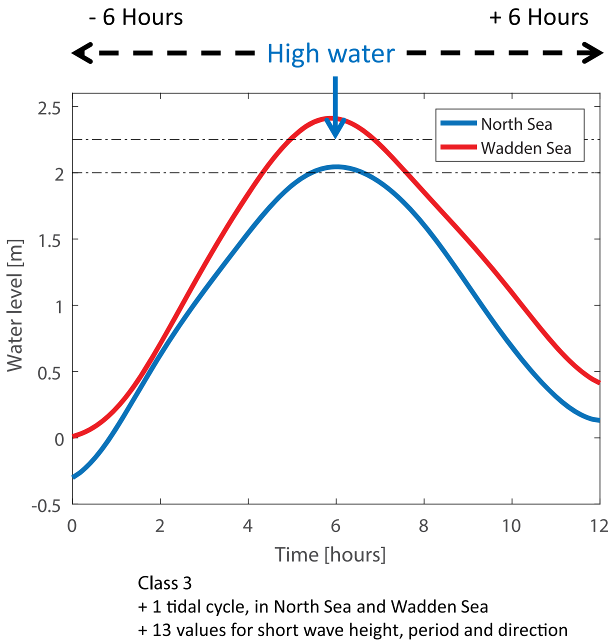

Figure 5. Diagram to illustrate the definition of the inundation classes. The water level curves act as an example of how the inundation classes are defined. This example belongs to class 3, based on the peak water level in the North Sea. This means that, for the final averaging, class 3 gains one tidal cycle in the North Sea and Wadden Sea, and 13 hourly values of the short wave height, peak period and wave direction. [Colour figure can be viewed at wileyonlinelibrary.com]

row during one storm. For every inundation event a tidal cycle of 12 h is obtained from the North Sea water level data, with the peak water level in the centre of the time series. Finally, all the individual events in one specific class are averaged to create a representative water level curve per class.

In addition, for every inundation event a tidal cycle for the same time frame is constructed in the Wadden Sea (station Schiermonnikoog). Since the classes are initially not based on the peak water level in the Wadden Sea, the peak water level in the Wadden Sea is not necessarily in the centre of the water level curve, as there is often a phase difference between the North Sea and Wadden Sea. Besides, the peak water level in the Wadden Sea can be higher than its specific class. For the Wadden Sea, the individual events per class are averaged as well.

In addition to the water levels, the offshore wave data are analyzed and used for the inundation classes (wave buoy Schiermonnikoog Noord). For every inundation event for the 25 years that are analyzed, 13 values in the same time frame (i.e. one per hour) for the significant short wave height, average short wave period and wave direction are added to one specific class. In total, one class contains $n = 13 \times m$ values of the above mentioned parameters, where m is the number of inundation events in one class and n is the total number of values. The representative values for those parameters are calculated using Eqs. (3), (4) and (5), respectively:

$$H_s = \sqrt{\frac{\sum_{i=1}^{n} H_{s,i}^2}{n}} \tag{3}$$

$$T_p = \frac{\sum_{i=1}^{n} (H_{s,i}^2 * T_{p,i})}{\sum_{i=1}^{n} H_{s,i}^2} \tag{4}$$

$$D = \frac{\sum_{i=1}^{n} (H_{s,i}^2 * D_i)}{\sum_{i=1}^{n} H_{s,i}^2} \quad (5)$$

Here, H_s is the significant short wave height, T_p the average wave period and D the wave direction. In this way, T_p and D are weighted with their energy ($\sim H_s^2$) and the weighted mean is calculated. Those values are then used to create a JONSWAP spectrum for each inundation class. For the JONSWAP spectra, the values for the peak enhancement factor γ and the directional spreading σ are 3.3 s^{-1} and 18°, respectively. We are not able to find a trend in the offshore wave forcing during one inundation event (e.g. larger waves during high water). Therefore, the wave forcing per inundation class is constant but varied between different classes.

Results: Model Validation

The model–data comparison shows good agreement, which is illustrated with all the r^2 and bias values (Table I) and the scatter plots at the instruments PT5 and ADV2, close to the beach crest (Figure 6). The results show that both the short wave height and the water depth, which contains the tide, storm surge and wave set-up, have very high r^2 values (ranging from 0.86 to 0.96), which means that the trend is accurately simulated. The positive bias shows that the water depth and short wave heights offshore from the beach crest (i.e. around PT4–PT5) are somewhat overpredicted. Further onshore, there is a bias towards negative values, but the r^2 values remain high. The IG wave height shows low r^2 values and a negative bias at the offshore part of the island. However, closer to the beach crest, the r^2 increases and the bias is close to zero, which means that the development of IG waves across the island is predicted accurately. The flow velocity at the beach crest (i.e. ADV2) is, although overpredicted with a bias of 0.16 m s^{-1}, also simulated sufficiently (r^2 of 0.63). Both the

Table I. Squared correlation coefficients (r^2) and bias for the water depths, short and IG wave heights and flow velocities for all instruments

	Water depth (m)		Short wave height (m)		IG wave height (m)		Flow velocity (m s^{-1})	
	r^2	Bias	r^2	Bias	r^2	Bias	r^2	Bias
PT1	0.94	0.13	0.92	0.19	0.37	−0.11		
PT2	0.90	0.14	0.86	0.26	0.27	−0.07		
PT3	0.92	0.07	0.87	0.14	0.38	−0.04		
PT4	0.92	0.14	0.87	0.10	0.54	−0.04		
PT5	0.92	0.09	0.87	0.08	0.70	−0.02		
PT6	0.95	0.02	0.89	0.07	0.76	−0.02		
PT7	0.95	−0.01	0.91	0.02	0.84	−0.02		
PT8	0.96	−0.06	0.91	−0.02	0.85	−0.03		
PT9	0.96	−0.02	0.91	−0.05	0.85	−0.03		
PT10	0.96	−0.06	0.89	−0.11	0.87	−0.04		
ADV2							0.63	0.16
ADV3							0.47	0.19

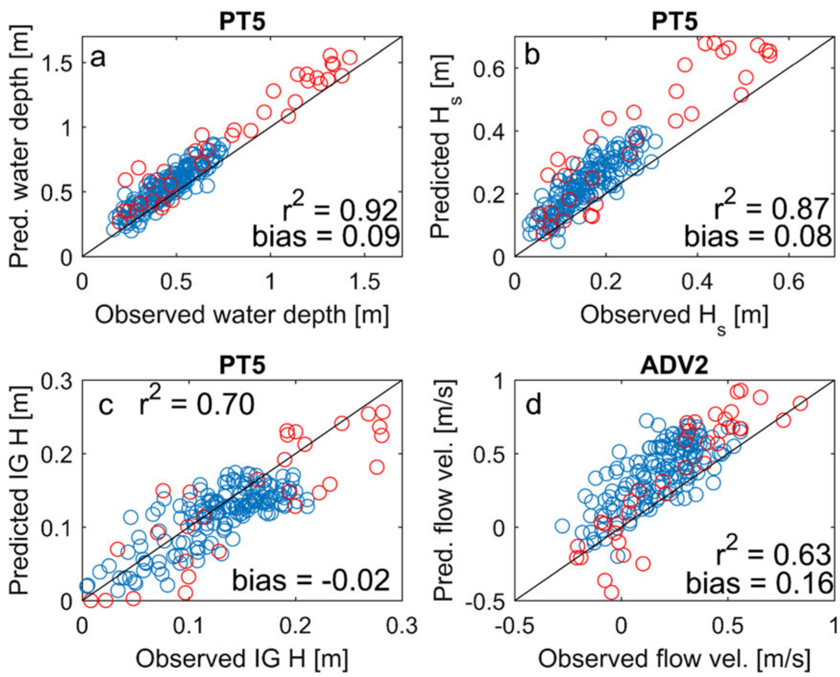

Figure 6. Observed versus predicted mean parameters for all inundations, for PT5 and ADV2. The black lines indicate the 1:1 position. The red circles are the two inundation events that are used for further analysis in Figure 7. (a) Water depth. (b) Short wave height. (c) IG wave height. (d) Flow velocity. [Colour figure can be viewed at wileyonlinelibrary.com]

observed and the predicted flow velocities result in positive as well as negative velocities, while the latter is only observed during some of the falling tides when the water level at the Wadden Sea side is higher.

To analyse the model–data comparison of the water depths, short- and IG wave heights in more detail, the variation of the mean parameters in a cross-shore direction during high tide is investigated for two inundation events (Figure 7). The first two tidal cycles of Figure 4 are chosen, which are indicated by the red colour in Figure 6. The first one represents the majority of the 11 inundation events, with peak water levels around 2 m in the North Sea, and the second one is the largest flooding event, with a peak water level in the North Sea of 2.7 m. Water depths are represented very accurately, for both inundations. Short wave heights are slightly overestimated at the offshore part of the island, especially for the large flooding. From PT7–PT8, the observed short wave height increases again in an onshore direction. This is probably caused by waves entering the island tail from the Wadden Sea side, which is not included in this model, and results in the negative bias for this part of the island (Engelstad *et al.*, 2017). The IG waves are underestimated for the offshore part of the island, both for the large as well as for the smaller inundation. However, closer to the beach crest the negative bias becomes less pronounced and the development of the IG waves in a cross-shore direction is predicted accurately.

Although we consider the biases to be small enough, it is useful to discuss the source of the deviations between model output and data. Firstly, it was found by Hoonhout and van Thiel de Vries (2012) that short wave heights tend to be overestimated by the model on shallow and gently sloping foreshores. Furthermore, the overestimation of the currents can possibly be related to the positive bias of both short waves and water depths. Moreover, the currents are measured at a certain height above the bed, whereas the model values are depth-averaged, which can result in a discrepancy between data and model output. Except for model issues, uncertainties could have been introduced by using the water level stations in the North Sea and Wadden Sea, and the wave buoy in the North Sea. Those locations are not exactly in line with our cross-shore profile, which can cause somewhat deviating model results.

Results: Long-Term Sediment Transport

Inundation classes

The water levels in the North Sea and Wadden Sea that are incorporated in the inundation classification are a combination of tide and storm surge (Figure 8), and they reveal two interesting trends. Firstly, the water level in the Wadden Sea lags behind the water level in the North Sea, which is probably a tide-induced effect as it also occurs during calm weather conditions. This results in higher water levels in the Wadden Sea than in the North Sea during the falling stages of the tide. Secondly, storm surges result in a larger increase of the mean water level in the Wadden Sea than in the North Sea side for larger storms and result in a smaller phase lag. As a result, only during part of the rising tide are water levels in the North Sea higher than in the Wadden Sea, whereas for the rest of the time Wadden Sea water levels are higher. The reverse of the water level gradient from North Sea to Wadden Sea occurs earlier as storms become more severe. For class 6, the water level in the Wadden Sea is higher than in the North Sea in deep water for the entire tidal cycle.

The wave forcing increases as expected with increasing storm magnitude (Table II). The offshore wave direction gradually changes from 304° to 317° N, concurrent with the change in wind direction that generated the storm surge. The frequency of occurrence exponentially decreases with increasing peak water levels. For example, class 1 occurs 23 times per year, whereas class 6 occurs only 0.3 times per year.

Processes per inundation class

Field observations and model results both indicate that the duration of overwash during storms, compared to the duration of inundation, is very limited due to the large tidal range, and the low profile at the chosen location. As a consequence, model simulations also suggest that sediment transport in the overwash phase only has a small contribution to the total transport during a flooding event (less than 1% of the total transport during one inundation event). Therefore, the analysis of the model results will focus on the inundation phase rather than the overwash phase.

The storms of the six inundation classes (Figure 9a) have a profound effect on the relevant hydrodynamic processes and the resulting sediment transport over the beach crest (Figure 9b–f, where positive means in the onshore, Wadden Sea direction and negative means in the offshore, North Sea direction). For every class, short wave heights peak during high water, when the water depth is largest (Figure 9b). For IG wave heights, this is less clear (Figure 9c). During the inundation phase, they stay more or less constant for several hours. The maximum values are larger with increasing inundation class for both short- and IG wave heights, because higher classes have larger water depths (less energy dissipation) and larger offshore waves.

Flow velocities (Figure 9d) demonstrate similar trends for all inundation classes during the rising tide. Flow is in the positive direction (i.e. towards the Wadden Sea). Furthermore, the positive peak typically occurs a few hours before high water and slightly increases in magnitude for higher classes. This peak occurs earlier for higher inundation classes. Both the magnitude and timing of the flow velocity peak are the result of a complex interplay between the water level dynamics in the North Sea and Wadden Sea, which is the combination of tide, storm surge and wave set-up (see conceptual model in Engelstad *et al.*, 2017). The earlier flow velocity peak for higher classes is mainly determined by the fact that the water level in the Wadden Sea exceeds the water level in the North Sea in an earlier stage. For lower classes, the phase difference results in higher water levels in the North Sea during rising tide. For higher classes the higher water levels in the Wadden Sea become more dominant, which results in the earlier flow velocity peak. The magnitude of the peak tends, on one hand, to decrease for higher classes because of the larger mean water level in the Wadden Sea. On the other hand, it tends to increase because of the larger wave set-up (larger waves result in more wave breaking), which increases the hydraulic gradient across the profile. The combined effect is that the magnitude of the flow velocity peak only slightly increases from class 1 to class 6.

During falling tide, the flow velocity gradually decreases to zero under the influence of the higher water level in the Wadden Sea. For the higher classes, the direction of the flow velocity even reverses, especially for classes 5 and 6. For class 6, this flow reversal already takes place before high tide. However, the magnitude of the negative flow velocity is significantly smaller than the positive values during rising tide. This is probably a result of the wave set-up that increases

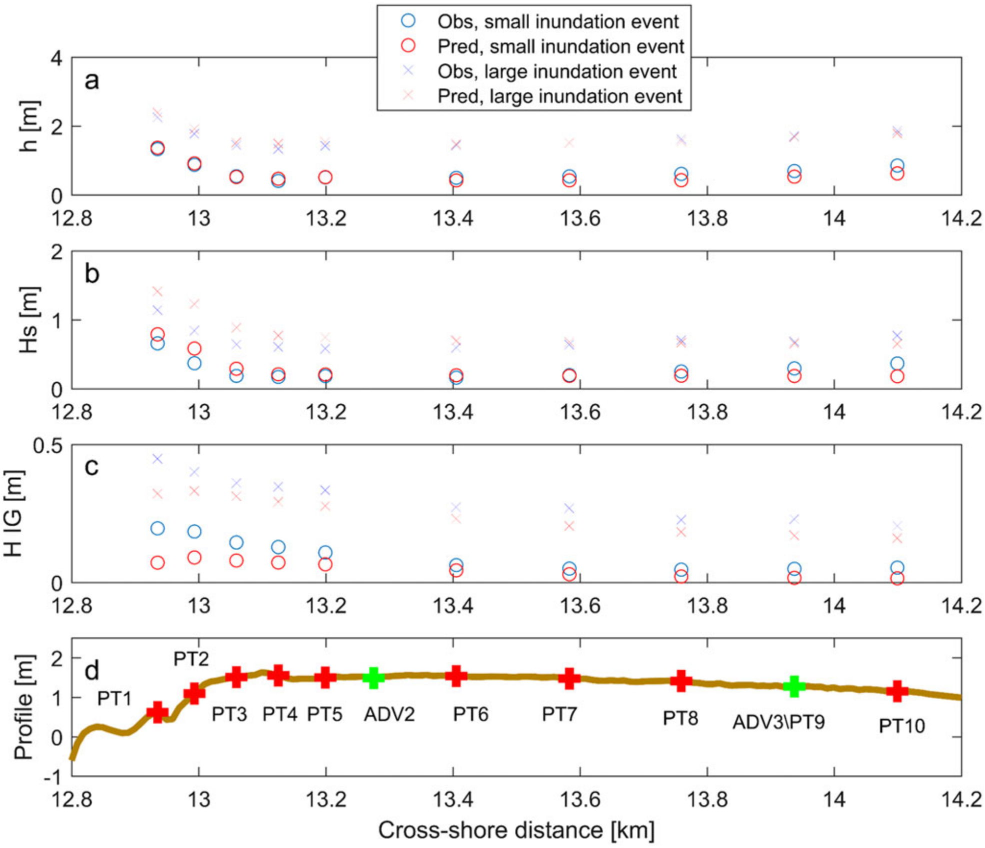

Figure 7. Observed and predicted (a) water depth, (b) short wave height and (c) IG wave height for all PTs at (d) the island part of the cross-shore profile. All values are averaged over 15 min. The circles represent one of the smaller inundation events and the crosses show the large inundation event (i.e. the middle tidal cycle in Figure 4). [Colour figure can be viewed at wileyonlinelibrary.com]

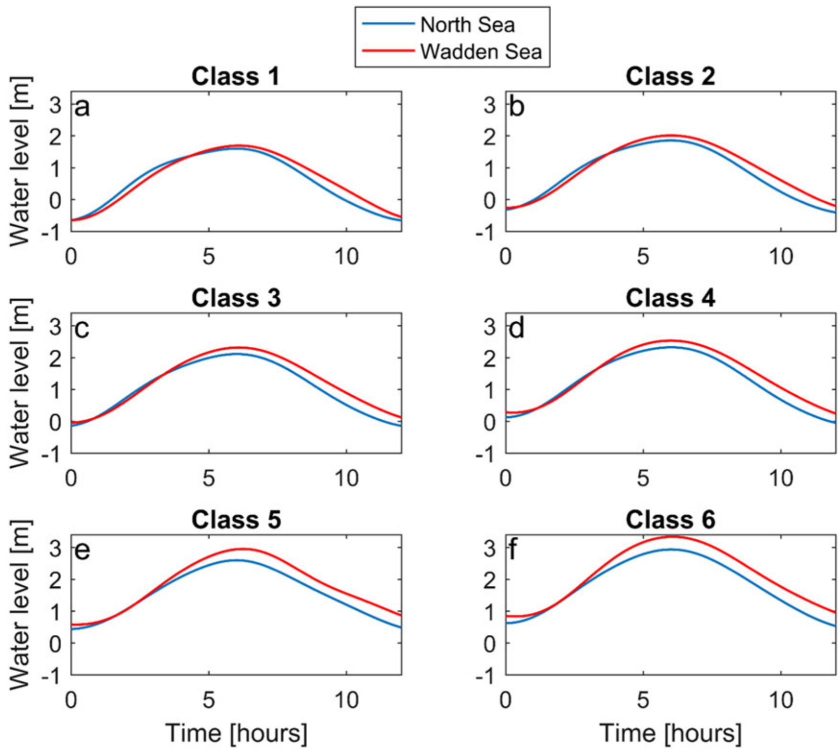

Figure 8. Water level curves used as boundary conditions for each class. Red is station Schiermonnikoog (Wadden Sea); blue is station Huibertgat (North Sea). [Colour figure can be viewed at wileyonlinelibrary.com]

Table II. Hydrodynamic conditions per class: peak water level; significant wave height; wave period; wave direction (270 = W, 360 = N); angle with shore; occurrence per year, based on 25 years of data

Class	Peak water level (m)	H_s (m)	Wave period (s)	Wave direction (° N)	Angle with shore (°)	Occurrence (per year)
1	1.50 < wl < 1.75	2.61	6.29	304	46	23.0
2	1.75 < wl < 2.00	3.42	6.97	306	44	7.4
3	2.00 < wl < 2.25	3.98	7.34	306	44	2.6
4	2.25 < wl < 2.50	4.33	7.69	307	43	0.8
5	2.50 < wl < 2.75	5.38	8.53	314	36	0.5
6	2.75 < wl	5.61	9.08	317	33	0.3

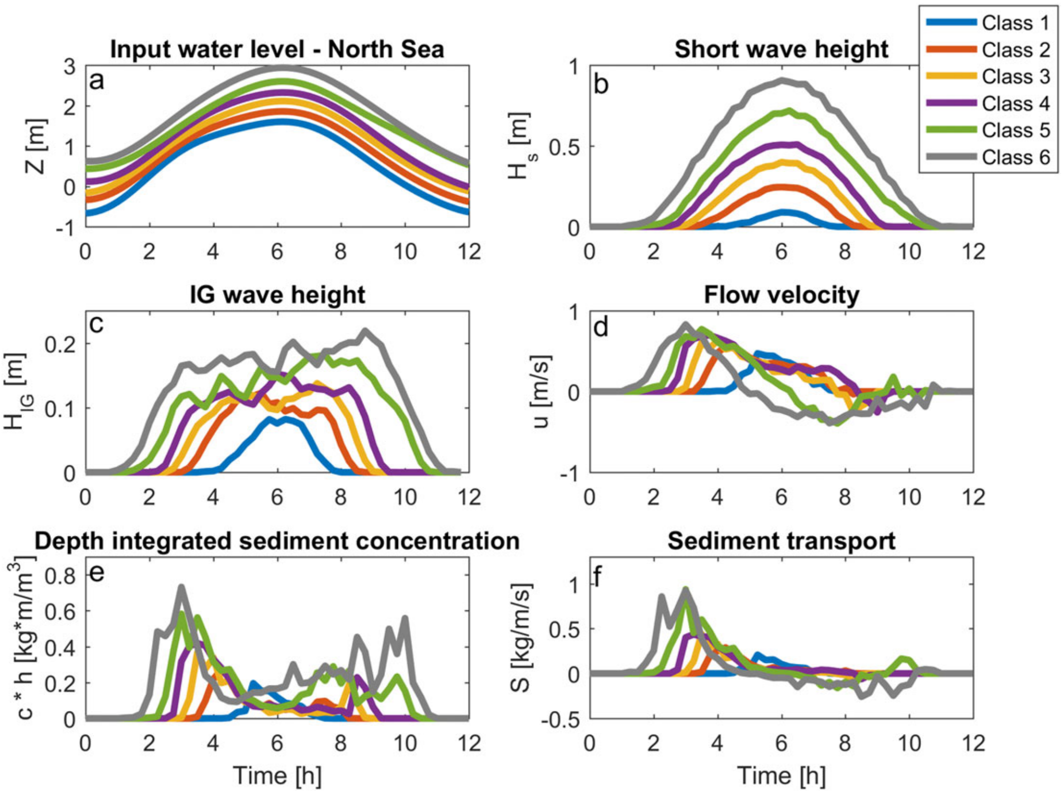

Figure 9. (a) Input North Sea water level curves. These are the same as in Figure 8. (b–f) Output of all inundation classes as a function of time, averaged over 15 min and calculated at the beach crest. (b) Short wave height. (c) IG wave height. (d) Cross-shore flow velocity. Positive is in the direction of the Wadden Sea. (e) Depth-integrated sediment concentration. (f) Sediment transport. Positive is in the direction of the Wadden Sea. [Colour figure can be viewed at wileyonlinelibrary.com]

the hydraulic gradient during rising tide, but decreases the reversed hydraulic gradient during falling tide.

Sediment can be stirred from the bed by short waves, IG waves and by currents. The depth-integrated sediment concentration, which is dominated by suspended load transport (Figure 9e), partly correlates with the flow velocity, both during rising tide and falling tide. In more detail, two concentration peaks arise, while the time in between the sediment concentration is much smaller, which is in phase with the flow reversal (i.e. when it is close to zero). However, especially the larger classes show that the concentration is not completely zero during the flow reversal, which implies also that the short waves and/or the IG waves stir sediment from the bed. Furthermore, the second concentration peak during falling tide is not always at the same time as the negative velocity peak. For example, the second concentration peak of class 6 is approximately 2 h later than the negative flow velocity peak. This suggests that the concentration also depends on the water level (i.e. less sediment stirring in deeper water).

Generally, suspended sediment transport (Figure 9f) is a function of flow velocity and depth-integrated sediment concentration. Therefore, the simulations show a strong correlation with the flow velocity during rising tide, with peak values that are higher and occur earlier for higher classes. During falling tide, sediment transport is negative for class 5 and 6, but is relatively small for all classes. This is caused by the negative flow velocities, which are close to or lower than the flow velocity threshold for sediment stirring.

Net sediment transport per inundation class

To investigate the effect of different inundation classes on the net sediment transport across the beach crest, the net transport is calculated as the positive transport during rising tide minus the negative transport during falling tide. It appears that the net sediment transport is always positive, towards the Wadden Sea (Figure 10, blue bars). Furthermore, it increases from class to class until class 5, which means that the factors that tend to increase the transport (e.g. higher water level, larger waves) are more important than the relatively higher water level in the Wadden Sea. However, from class 5 to class 6 the transport

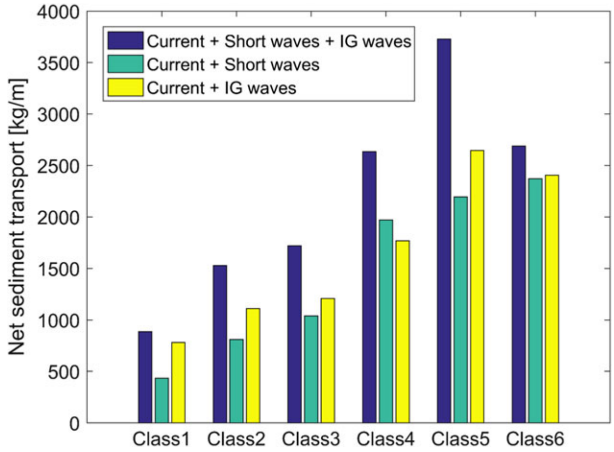

Figure 10. Net sediment transport for all classes at the beach crest, for the entire tidal cycle. The blue bars contain all sediment stirring mechanisms (i.e. short waves, IG waves and the cross-shore current). The green and yellow bars miss one component. [Colour figure can be viewed at wileyonlinelibrary.com]

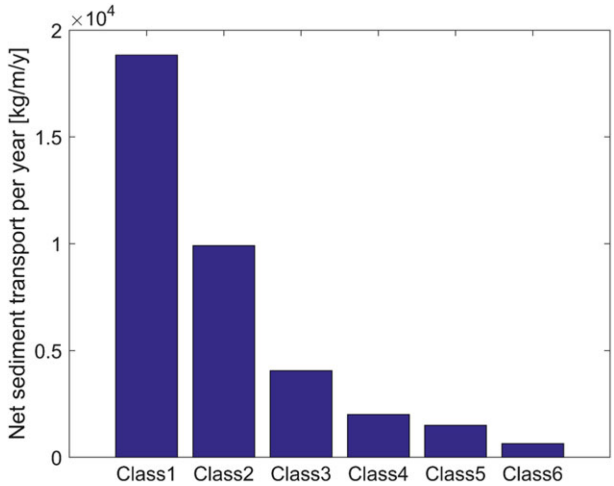

Figure 11. Total sediment transport per year at the beach crest. Compared to the blue bars in Figure 10, the net transport is multiplied by the average number of storms per year in each class, defined in Table II. [Colour figure can be viewed at wileyonlinelibrary.com]

decreases, which is mainly an effect of the falling tide phase of the inundation events. During rising tide the net onshore transport is slightly larger for class 6, but during falling tide there is more offshore transport for class 6 as well.

The same inundation classes are simulated two more times by excluding once the short wave stirring and the other time the IG wave stirring. Note that only the sediment stirring is adapted, not the wave itself. For example, when the short wave sediment stirring is excluded, the short waves still influence the hydraulic gradient by creating wave set-up. More details can be found in the Appendix. Excluding the sediment stirring by short waves or IG waves decreases the net sediment transport at the beach crest; however, an important part is stirred by the current (Figure 10). From class 5 to class 6, the simulations without sediment stirring by the IG waves show an increase in net transport, whereas it decreases for the default simulations. This indicates that this decrease for the default simulations is mainly caused by sediment that is stirred by the IG waves and transported in the North Sea direction by the current, during falling tide.

Net transport over the beach crest is four to five times larger for high inundation classes than for class 1 events; however, if net transport is combined with the frequency of occurrence (based on 25 years) the total cumulative transport is largest for less severe storms. Class 1 inundation events (peak water levels between 1.50 and 1.75 m) typically occur several times a year, for example when a small storm surge coincides with spring tide. Class 5 and 6 (peak water levels higher than 2.50 m) are relatively exceptional NW storms that occur less than once a year. Therefore, the frequency of occurrence from class 1 to class 5–6 decreases by one to two orders of magnitude. When the net sediment transport of each inundation class is multiplied by the frequency of occurrence, the larger net sediment transport during larger storms is not enough to compensate for their lower frequency of occurrence and to make these storms the most dominant ones in terms of net sediment transport (Figure 11). This implies that those frequently occurring inundation events have to be taken into account when the potential contribution of inundation events to the long-term vertical accretion of the Wadden Islands is investigated.

Discussion

XBeach performance

We were able to validate the hydrodynamic settings of an XBeach model under overwash and inundation regimes. Despite a gamma value of 0.45 in the wave breaking formulation, the short wave heights and water depths, and therefore the flow velocities as well, are still slightly overestimated. On the other hand, the simulated IG wave heights are slightly underestimated, especially offshore. This is in line with other studies that compared the hydrodynamic processes in XBeach with field data or lab experiments (Hoonhout and van Thiel de Vries, 2012; de Winter *et al.*, 2015). Our results are probably slightly influenced by this bias, especially the relative role of currents and waves on sediment stirring. However, this mainly influences the amount of sediment transport, but does not change our conclusion that gentle, weaker storms have more impact on the long-term, cumulative transport than the large, less frequent storms.

Overwash and inundation at the island tail of Schiermonnikoog

The sediment transport is only weakly increasing for higher inundation classes, which is related to the effect of the reversed flow in offshore direction during falling tides. This is investigated in more detail with a new set of simulations, where for every inundation class the prescribed water levels at the North Sea and Wadden Sea boundary are the same; hence no time lags and storm surge differences are considered. In this scenario, the hydraulic gradient across the island is solely determined by the wave set-up. Sediment transport is then only in the Wadden Sea direction. Comparing Figures 12 and Figure 9f clearly demonstrates that the higher mean water level in the Wadden Sea during storms has a strong impact on the net sediment transport over the beach crest. The total transport during an inundation event is much smaller in the original simulations than in the simulations with equal water level in the North Sea and Wadden Sea, ranging from a decrease of 20% to 90% from class 1 to class 6. The important role of the back-barrier basin when it is connected with the ocean or sea during inundation is also recognized in other studies, for example by Harter and Figlus (2017), Hoekstra *et al.* (2009), Sherwood *et al.* (2014) and de Vet *et al.* (2015). Sherwood *et al.* (2014) also found reversed currents as a result of higher back-barrier water levels for the Chandeleur Islands in Louisiana, while Hoekstra *et al.* (2009) concluded as well

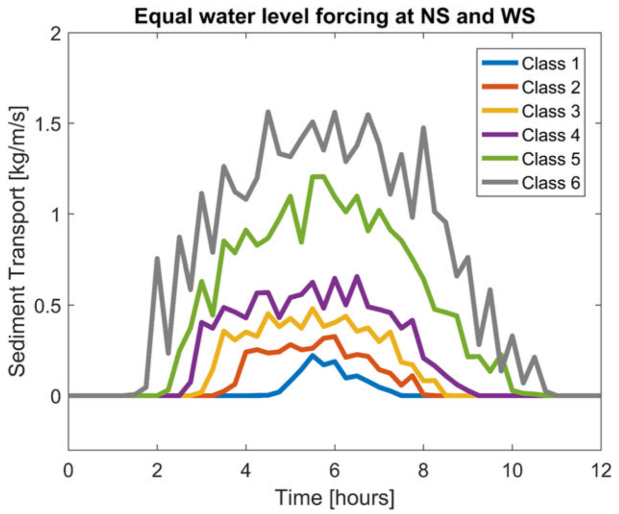

Figure 12. Sediment transport at the beach crest, without the hydraulic gradient caused by storm surges and tidal phase differences. Therefore, sediment transport is always in the Wadden Sea direction. [Colour figure can be viewed at wileyonlinelibrary.com]

that water can reach Schiermonnikoog from both sides of the island.

The inundation events at the low-lying island tail (i.e. a beach crest of 1.6 m) undergo all four stages of the regime of Sallenger (2000). The occurrence and duration of the inundation phase in general are mainly determined by the combination of beach or dune crest height and the mean water level. Obviously, inundation is always preceded by an overwash phase during rising tide. However, at this specific field site, the duration of the overwash phase is very short compared to the duration of the inundation phase. In addition, results have also shown that the cross-shore current during inundation, induced by water level gradients between the North Sea and Wadden Sea and by wave set-up, is one of the most dominant mechanisms for sediment stirring and transport across the island (Figure 10). Consequently, the net sediment transport across the beach crest during overwash is one or two orders of magnitude smaller than the transport during inundation at this specific location, which leads to the conclusion that the overwash phase plays a minor role in the net sediment transport across the island tail of Schiermonnikoog. This is in line with the findings of Harter and Figlus (2017), who concluded that the currents during the inundation regime lead to more bed level change than the wave overtopping during the overwash regime at Follet's Island, Texas, based on their XBeach simulations. However, the main difference between our study site and the location of many other studies (e.g. McCall *et al.*, 2010) is the absence of dunes, the low level of the beach crest and the mesotidal conditions.

Another difference between our field site and other barrier systems related to the very low-lying beach crest is the importance of smaller, frequently occurring storms compared to larger and more exceptional storms for the long-term cumulative sediment transport. Other studies investigating barriers with a higher beach or dune crest often tend to focus on these severe storms because they are needed to create significant dune erosion or even breaching before inundation occurs. Examples are the work of Morton and Sallenger (2003) and Nielsen and Nielsen (2006), which described a large storm in 1990 that caused a breach at the dunes of Skallingen, Denmark. Our research shows that for typical Wadden Island conditions, where washover openings already exist, also the more frequently occurring inundation events should be taken into account for the analysis of the long-term sediment budget.

The Schiermonnikoog island tail versus the 2D washover openings

Typically, under natural conditions the dune rows at the Wadden Islands are not closed over the full length of the island and have natural gaps, so-called washover openings. During storms, when critical water levels are exceeded, water and sediment can flow across the island via these openings. To protect the Wadden Islands from flooding, artificial sand-drift dikes that close these gaps were constructed in previous centuries (Oost *et al.*, 2012). Sediment transport across the island caused by overwash and inundation is thus significantly reduced. Therefore, the areas located directly behind the dunes tend to become lower lying relative to rising sea level. At Schiermonnikoog, a large storm in 1973 partly destroyed the sand-drift dike, which created the current openings, but these are much smaller than the natural openings before the sand-drift dike was built.

Recently, in the Netherlands, the reactivation of the washover openings was considered by nature organizations to stimulate sediment deposition behind the dunes. An additional advantage of this would be the development of a more dynamical ecosystem. Our study contributes to the knowledge that is required to make this decision; however, potential differences between the 1D island tail and the 2D washover openings have to be considered. The first difference between those locations is the beach crest or washover crest height (Figure 2). Many washover openings are 20–30 cm higher than the beach crest at the island tail. At first sight this seems to be a small difference; however, this would mean that the class 1 inundation events, which in the long term lead to the most sediment transport at the island tail, do not occur at the washover openings. Furthermore, 2D effects must be taken into account at those locations. For example, flow contraction through an opening can accelerate currents, which enhances sediment transport. Sediment slumping from the side walls of the dunes can affect the sediment transport as well and deposition patterns behind the dunes can vary in the alongshore direction. The influence of these properties of the 2D washover openings on the hydrodynamics, sediment transport and morphology change will be investigated in future studies.

Conclusions

In this paper we study the influence of overwash and inundation events on the hydrodynamics and sediment transport across the low-lying Wadden Islands under mesotidal conditions. Firstly, the model XBeach is validated with field data gathered at the barrier island tail of Schiermonnikoog, the Netherlands, during overwash and inundation events. Water depths and short wave heights across the island are simulated accurately with r^2 values of 0.85 and higher, and a small positive bias. IG wave heights are slightly underestimated. Cross-shore flow velocities result in somewhat lower but still sufficient r^2 values and a slightly higher bias. We conclude that the model–data comparison is robust enough to use the model for further analysis. Secondly, we use XBeach to simulate the cross-shore sediment transport for a wide range of waves, tides and storm surge conditions. Tidal phase differences and storm surge dynamics result in higher water levels in the Wadden Sea compared to the North Sea. This is a crucial aspect for the sediment transport across the island tail, resulting in a smaller or even reversed current and a reduced net sediment transport. Over a tidal cycle, the net sediment transport direction is still towards the Wadden Sea. We conclude that the cumulative effect of relatively mild storms is more important for the long-term sediment transport than the cumulative effect of large, more exceptional North Sea storms. Per storm, more sediment is transported across the island when the magnitude of the storm increases. However, combined with the decreasing frequency of occurrence of larger storms, we conclude that exceptional storms in mesotidal settings are not crucial for the potential vertical accretion of the island tails during overwash and inundation events.

Acknowledgements— We would like to thank Marcel van Maarseveen, Henk Markies, Chris Roosendaal and Arjan van Eijk for their technical support during the field campaign. Without them, it would not have been possible. We would also like to thank Natuurmonumenten for help during the fieldwork. Daan Wesselman is supported by Climate-KIC. Anita Engelstad is supported by the Netherlands Organisation for Scientific Research (NWO), as well as by Natuurmonumenten, the National Forest Service (Staatsbosbeheer) and the Wadden Academy.

References

Androulidakis YS, Kombiadou KD, Makris CV, Baltikas VN, Krestenitis YN. 2015. Storm surges in the Mediterranean Sea: Variability and trends under future climatic conditions. *Dynamics of Atmospheres and Oceans* **71**: 56–82.

Battjes JA. 1974. *Surf similarity*: Copenhagen, 466–480.

Beach RA, Sternberg RW. 1988. Suspended sediment transport in the surf zone: Response to cross-shore infragravity motion. *Marine Geology* **80**: 61–79.

de Bakker ATM, Tissier MFS, Ruessink BG. 2015. Beach steepness effects on nonlinear infragravity–wave interactions: A numerical study. *Journal of Geophysical Research: Oceans* **121**: 554–570.

de Vet PLM, McCall RT, den Bieman JP, Stive MJF, van Ormondt M. 2015. *Modelling dune erosion, overwash and breaching at fire island (NY) during hurricane sandy, Proceedings of the Coastal Sediments, 2015*: San Diego, CA.

de Winter R, Gongriep F, Ruessink B. 2015. Observations and modeling of alongshore variability in dune erosion at Egmond aan Zee, the Netherlands. *Coastal Engineering* **99**: 167–175.

Donnelly C, Kraus NC, Larson M. Coastal overwash. Part 1 Overview of processes, ERDC/RSM-TN-14, U.S. Army Engineer Research and Development Center, Vicksburg, MS, 2004.

Donnelly C, Kraus N, Larson M. 2006. State of knowledge on measurement and modeling of coastal overwash. *Journal of Coastal Research* **22**: 965–991.

Engelstad A, Ruessink BG, Wesselman D, Hoekstra P, Oost A, van der Vegt M. 2017. Observations of waves and currents during barrier island inundation. *Journal of Geophysical Research* **122**: 3152–3169.

FitzGerald D, Kulp M, Hughes Z, Georgiou I, Miner M, Penland S, Howes N. 2007. Impacts of rising sea level to backbarrier wetlands, tidal inlets, and barrier islands: Barataria Coast, Louisiana. *Proceedings of Coastal Sediments* **7**: 1179–1192.

Flato G, Marotzke J, Abiodun B, Braconnot P, Chou SC, Collins W, Cox P, Driouech F, Emori S, Eyring V, Forest C, Gleckler P, Guilyardi E, Jakob C, Kattsov V, Reason C, Rummukainen M. 2013. Evaluation of climate models. In *Climate Change 2013: The Physical Science Basis. Contribution of Working Group I to the Fifth Assessment Report of the Intergovernmental Panel on Climate Change*, Stocker TF, Qin D, Plattner GK, Tignor M, Allen SK, Boschung J, Nauels A, Xia Y, Bex V, Midgley PM (eds), Cambridge University Press: Cambridge, United Kingdom and New York, NY, USA.

Harter C, Figlus J. 2017. Numerical modeling of the morphodynamic response of a low-lying barrier island beach and foredune system inundated during Hurricane Ike using XBeach and CSHORE. *Coastal Engineering* **120**: 64–74.

Hayes MO. 1979. Barrier island morphology as a function of tidal and wave regime. In *Barrier Islands*, Leatherman S (ed), from the Gulf of St Lawrence to the Gulf of Mexico: New York: Academic; pp. 1–27.

Herbers THC, Elgar S, Guza RT. 1994. Infragravity-frequency (0.005–0.05 Hz) motions on the shelf. Part I. Forced waves. *Journal of Physical Oceanography* **24**: 917–927.

Hoekstra P, ten Haaf M, Buijs P, Oost A, Klein Breteler R, van der Giessen K, van der Vegt M. 2009. Washover development on mixed energy, mesotidal barrier island systems. *Coastal Dynamics* **83**: 25–32.

Holthuijsen LH. 2007. *Waves in Oceanic and Coastal Waters*. Cambridge University Press: Cambridge, UK.

Hoonhout B, van Thiel de Vries JSM. 2012. *Modelling dune erosion, overwash and inundation of barrier islands, Proceedings of the Conference on Coastal Engineering*: Santander.

Lapetina A, Sheng YP. 2015. Simulating complex storm surge dynamics: Three-dimensionality, vegetation effect, and onshore sediment transport. *Journal of Geophysical Research: Oceans* **120**: 7363–7380.

Lazarus ED. 2016. Scaling laws for coastal overwash morphology. *Geophysical Research Letters* **43**: 12113–12119.

Lazarus ED, Armstrong S. 2015. Self-organized pattern formation in coastal barrier washover deposits. *Geology* **43**: 363–366.

Leatherman SP. 1976. *Barrier island dynamics: Overwash processes and eolian transport*. ASCE: Reston, VA,1958–1974.

Leatherman SP. 1985. Geomorphic and stratigraphic analysis of Fire Island, New York. *Marine Geology* **63**: 173–195.

Longuet-Higgins MS. 1983. Wave set-up, percolation and undertow in the surf zone. *Proceedings of the Royal Society of London A* **390**: 283–291.

Longuet-Higgins MS, Stewart RW. 1962. Radiation stress and mass transport in gravity waves, with application to 'surf beats'. *Journal of Fluid Mechanics* **13**: 481–504.

Masselink G, van Heteren S. 2014. Response of wave-dominated and mixed-energy barriers to storms. *Marine Geology* **352**: 321–347.

Matias A, Ferreira Ó, Vila-Concejo A, Morris B, Dias J. 2009. Foreshore and hydrodynamic factors governing overwash. *Journal of Coastal Research* **1**: 636–640.

McCall R, De Vries JVT, Plant N, Van Dongeren A, Roelvink J, Thompson D, Reniers A. 2010. Two-dimensional time dependent hurricane overwash and erosion modeling at Santa Rosa Island. *Coastal Engineering* **57**: 668–683.

Morton RA, Sallenger AH. 2003. Morphological impacts of extreme storms on sandy beaches and barriers. *Journal of Coastal Research* **19**: 560–573.

Nielsen N, Nielsen J. 2006. Development of a washover fan on a transgressive barrier, Skallingen, Denmark. *Journal of Coastal Research Special Issue* **39**: 107–111.

Oost A, Hoekstra P, Wiersma A, Flemming B, Lammerts E, Pejrup M, Hofstede J, Van der Valk B, Kiden P, Bartholdy J, et al. 2012. Barrier island management: Lessons from the past and directions for the future. *Ocean and Coastal Management* **68**: 18–38.

Plant NG, Stockdon HF. 2012. Probabilistic prediction of barrier-island response to hurricanes. *Journal of Geophysical Research: Earth Surface* **117**.

Roelvink D, Reniers A, van Dongeren A, De Vries J, van T, McCall R, Lescinski J. 2009. Modelling storm impacts on beaches, dunes and barrier islands. *Coastal Engineering* **56**: 1133–1152.

Roelvink J. 1993. Dissipation in random wave groups incident on a beach. *Coastal Engineering* **19**: 127–150.

Sallenger AH. 2000. Storm impact scale for barrier islands. *Journal of Coastal Research* **16**: 890–895.

Schupp CA, Winn NT, Pearl TL, Kumer JP, Carruthers TJ, Zimmerman CS. 2013. Restoration of overwash processes creates piping plover (Charadrius melodus) habitat on a barrier island (Assateague Island, Maryland). *Estuarine, Coastal and Shelf Science* **116**: 11–20.

Sherwood CR, Long JW, Dickhudt PJ, Dalyander PS, Thompson DM, Plant NG. 2014. Inundation of a barrier island (Chandeleur Islands, Louisiana, USA) during a hurricane: observed water-level gradients and modeled seaward sand transport. *Journal of Geophysical Research: Earth Surface* **119**: 1498–1515.

Stockdon H, Thompson D, Plant N, Long J. 2014. Evaluation of wave runup predictions from numerical and parametric models. *Coastal Engineering* **92**: 1–11.

Van Dusen BM, Theuerkauf EJ, Fegley SR, Rodriguez AB. 2016. Monitoring overwash using water-level loggers resolves frequent inundation and run-up events. *Geomorphology* **254**: 32–40.

van Rijn LC. 2007. Unified view of sediment transport by currents and waves. II. Suspended transport. *Journal of Hydraulic Engineering* **133**: 649–667.
Van Thiel de Vries JSM. 2009. *Dune Erosion during Storm Surges*, doctoral thesis, TU Delft.
Walstra D, Roelvink J, Groeneweg J. 2000. *Calculation of wave-driven currents in a 3D mean flow model*: Sydney, Australia,1050–1063.
Williams H. 2015. Contrasting styles of Hurricane Irene washover sedimentation on three east coast barrier islands: Cape Lookout, North Carolina; Assateague Island, Virginia; and Fire Island, New York. *Geomorphology* **231**: 182–192.

Appendix

This appendix describes the governing XBeach equations that compute the hydrodynamics and sediment concentration and transport. All details can be found in Roelvink *et al.* (2009). For this study we use the 1D cross-shore variant of the surf beat mode. Therefore, we only describe the cross-shore terms in the equations. Furthermore, we leave out the terms that are not used here. In the surf beat mode, the short waves are solved with the wave action balance on the scale of wave groups. The infragravity waves and mean flows are then computed with the shallow-water equations. The sediment transport is calculated with an advection–diffusion equation, while the equilibrium sediment concentration is derived with the Van Thiel–Van Rijn equation.

Short wave action

Wave forcing is computed with a time-varying version of the wave action balance (Eq. (A1)):

$$\frac{\partial A}{\partial t} + \frac{\partial c_{g,x} A}{\partial x} + \frac{\partial c_\theta A}{\partial \theta} = -\frac{D_w}{\sigma} \tag{A1}$$

where $c_{g,x}$ and c_θ is the wave action speed in x and directional space, respectively. D_w is an energy dissipation term caused by wave breaking. σ is the intrinsic frequency and A is the wave action computed as

$$A(x, y, t, \theta) = \frac{S_w(x, y, t, \theta)}{\sigma(x, y, t)} \tag{A2}$$

where S_w is the wave energy density in each directional bin.

The wave breaking dissipation term is based on the extended Roelvink formula, where the fraction of breaking waves (Q_b) is multiplied by the dissipation per breaking event (Eqs. A3–A5):

$$D_w = 2\frac{\alpha}{T_{\mathrm{rep}}} Q_b E_w \frac{H_{\mathrm{rms}}}{h} \tag{A3}$$

$$Q_b = 1 - \exp\left[-\left(\frac{H_{\mathrm{rms}}}{H_{\max}}\right)^n\right],\ H_{\mathrm{rms}} = \sqrt{\frac{8E_w}{\rho g}},\ H_{\max} = \gamma\cdot(h + \partial H_{\mathrm{rms}}) \tag{A4}$$

$$E_w(x, y, t) = \int_0^{2\phi} S_w(x, y, t, \theta)\mathrm{d}\theta \tag{A5}$$

where α is a wave dissipation coefficient, T_{rep} is the representative wave period, E_w is the energy of the wave, H_{rms} and $H_{\max}$ are the root mean square and maximum wave height, respectively, and n and γ are free parameters. For this study, for γ a value of 0.45 instead of the default value of 0.55 is used.

Shallow-water equations

The infragravity waves and mean flows are calculated with the generalized Lagrangian mean (GLM) shallow-water equations (Walstra *et al.*, 2000). The Lagrangian velocities are related to the Eularian velocities and the Stokes drift:

$$u^L = u^E + u^S,\ v^L = v^E + v^S \tag{A6}$$

The 1D GLM-momentum equations are then

$$\frac{\partial u^L}{\partial t} + u^L\frac{\partial u^L}{\partial x} - \upsilon_h\left(\frac{\partial^2 u^L}{\partial x^2}\right) = -\frac{\tau_{bx}^E}{\rho h} - g\frac{\partial \eta}{\partial x} + \frac{F_x}{\rho h} \tag{A7}$$

$$\frac{\partial \eta}{\partial t} + \frac{\partial h u^L}{\partial x} = 0 \tag{A8}$$

where υ_h the horizontal viscosity, τ_{bx} is the bed shear stress, η is the water level and F_x is the wave-induced stress. The bed shear stress is calculated thus:

$$\tau_{bx}^E = c_f \rho u_E \sqrt{(1.16 u_{\mathrm{rms}})^2 + (u_E)^2} \tag{A9}$$

where c_f is the dimensionless friction coefficient and u_{rms} the wave orbital velocity.

Sediment transport

The sediment concentrations are computed using an advection–diffusion equation with a source–sink term based on the equilibrium sediment concentration:

$$\frac{\partial hC}{\partial t} + \frac{\partial hCu^E}{\partial x} + \frac{\partial}{\partial x}\left(D_h h\frac{\partial C}{\partial x}\right) = \frac{hC_{\mathrm{eq}} - hC}{T_s} \tag{A10}$$

where C is the depth-averaged sediment concentration (varying on the wave-group timescale), D_h is the sediment diffusion coefficient, T_s is an adaptation time related to the entrainment of sediment and C_{eq} is the equilibrium equation, computed with the Van Thiel–Van Rijn equation (van Rijn, 2007; Van Thiel de Vries, 2009):

$$C_{\mathrm{eq,b}} = \frac{A_{\mathrm{sb}}}{h}\left(\sqrt{v_{\mathrm{mg}}^2 + 0.64 u_{\mathrm{rms,2}}^2} - U_{\mathrm{cr}}\right)^{1.5} \tag{A11}$$

$$C_{\mathrm{eq},s} = \frac{A_{\mathrm{ss}}}{h}\left(\sqrt{v_{\mathrm{mg}}^2 + 0.64 u_{\mathrm{rms,2}}^2} - U_{\mathrm{cr}}\right)^{2.4} \tag{A12}$$

where $C_{\mathrm{eq,b}}$ and $C_{\mathrm{eq,s}}$ are the equilibrium concentration for bedload and suspended load, respectively, A_{sb} and A_{ss} are coefficients and U_{cr} is the critical velocity. v_{mg} is the flow velocity magnitude. When long wave stirring is turned on (lws = 1), v_{mg} is simply the magnitude of the Eulerian velocity:

$$v_{\mathrm{mg}} = \sqrt{(u^E)^2 + (v^E)^2} \tag{A13}$$

However, if lws = 0 then m_{mg} is calculated with two terms, a factor of v_{mg} of the previous time step and a current-averaged part, based on a factor f_{cats}:

$$v_{\mathrm{mg}}^n = \left(1 - \frac{\mathrm{d}t}{f_{\mathrm{cats}} T_{\mathrm{rep}}}\right) v_{\mathrm{mg}}^{n-1} + \frac{\mathrm{d}t}{f_{\mathrm{cats}} T_{\mathrm{rep}}}\sqrt{(u^E)^2 + (v^E)^2} \tag{A14}$$

This is in fact calculating the average over one wave period, so that wave stirring by the IG waves is excluded. When short wave stirring is turned on (sws = 1), Eqs. A11 and (A12) are used for determining the equilibrium concentration. However, when sws = 0, the term $0.64u_{rms,2}^2$ is left out of the equations.